

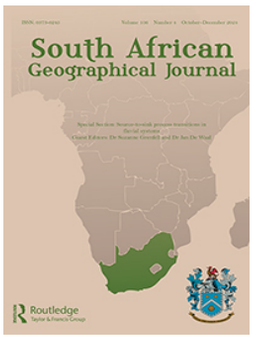
https://dspace.org/

Flood dynamics on teh upper Letaba River South Africa deduced from luminescence dating

Jasper Knight; Mary Evans

https://hdl.handle.net/10539/42204
WOS

Downloaded from a DSpace repository. https://dspace.org/



South African Geographical Journal

ISSN: (Print) (Online) Journal homepage: www.tandfonline.com/journals/rsag20

Flood dynamics on the upper Letaba River, South Africa, deduced from luminescence dating

Jasper Knight & Mary Evans

To cite this article: Jasper Knight & Mary Evans (2024) Flood dynamics on the upper Letaba River, South Africa, deduced from luminescence dating, South African Geographical Journal, 106:4, 423-445, DOI: 10.1080/03736245.2024.2333764

To link to this article: https://doi.org/10.1080/03736245.2024.2333764

Published online: 24 Mar 2024.

Submit your article to this journal

Article views: 106

View related articles

View Crossmark data

Citing articles: 2 View citing articles

Full Terms & Conditions of access and use can be found at
https://www.tandfonline.com/action/journalInformation?journalCode=rsag20

SOUTH AFRICAN GEOGRAPHICAL JOURNAL
2024, VOL. 106, NO. 4, 423–445
https://doi.org/10.1080/03736245.2024.2333764

Routledge
Taylor & Francis Group

Check for updates

Flood dynamics on the upper Letaba River, South Africa, deduced from luminescence dating

Jasper Knight and Mary Evans

School of Geography, Archaeology and Environmental Studies, University of the Witwatersrand, Johannesburg, South Africa

ABSTRACT

The Letaba River is one of several east-flowing rivers in the semiarid region of northeast South Africa. There is strong seasonality of river discharge and patterns of geomorphic behaviour along bedrock- and sediment-dominated reaches in these rivers, and in response to extreme seasonal flood events. This paper presents new luminescence ages on sediment samples from five sites in upper (headwater) reaches of the Letaba River catchment outside of Kruger National Park, South Africa, combined with evidence from reach-scale geomorphology and sediment sample analysis. River reaches are mainly mixed bedrock-alluvial with a patchwork of poorly sorted coarse sand bars overlying an abraded extended bedrock channel system. Luminescence ages from river sediment deposits ($n = 13$) cluster around three time periods of the last 400 years, 500–1100 BP, and 1400 BP. This suggests different reworked populations are present, which are a result of the partial bleaching of quartz grains and, thus, a mixed luminescence signal as flood-transported sediments are progressively moved from one depositional sink to another. This pattern of luminescence ages is quite different to lowland river systems in the same region where ages on the whole are significantly younger. Flood processes and dynamics in headwater reaches of semiarid rivers are often not considered but can yield a better understanding of system sensitivity to climate and event forcing.

ARTICLE HISTORY
Received 24 July 2023
Accepted 5 March 2024

KEYWORDS
Fluvial geomorphology; OSL dating; river floods; sediment reworking; semiarid rivers

1. Introduction

Seasonal rainfall and subsequent flooding are common drivers of geomorphic change on the semiarid rivers of southeastern South Africa (Heritage et al., 2001a, 2014, 2019; Rountree et al., 2000). High water velocities result in sediment erosion and depositional patterns that are manifested through changes in the distributions of (1) bare bedrock *versus* loose sand present across the flood-affected zone; (2) surface sediment types and properties such as grain size; and (3) fluvial landforms (Knight & Evans, 2022). These flood-driven geomorphic changes, related to the interplay between sediment deposition and the presence of bare rock surfaces, are particularly well demonstrated in river headwaters where both bedrock and a thin surficial cover of loose sediments are present, rather than in lower-reach

CONTACT Jasper Knight jasper.knight@wits.ac.za School of Geography, Archaeology and Environmental Studies, University of the Witwatersrand, Private Bag 3, Wits, Johannesburg 2050, South Africa

© 2024 The Society of South African Geographers

areas where sediment thickness is greater and where bedrock is commonly covered up (Baggs Sargood et al., 2015; Broadhurst & Heritage, 1998; Maswanganye et al., 2022; Wohl & Beckman, 2014). This may mean that the sediment dynamics of steeper headwater areas of rivers may be different to lower gradient reaches farther downstream (Thompson et al., 2007; Wohl & Beckman, 2014). However, there are very few studies that have considered headwater (mountainous) rivers in southern Africa, or their longitudinal sediment connectivity to their downstream reaches (Grenfell et al., 2014; Knight & Grab, 2018; Walsh et al., 2023).

Many studies globally have examined the dynamics of bedrock river systems, including the relative roles of geologic control *versus* floodwater processes in bedrock channel geomorphology (e.g. Johnson & Finnegan, 2015; Wohl & Beckman, 2014; Yanites, 2018). The dynamics of mixed bedrock – alluvial channels are more complex than bedrock systems alone because of the potential role of surficial sediments in protecting the underlying bedrock surface from erosion and in providing abraders for bedrock erosion (Toone et al., 2014; Baynes et al., 2020; Heitmuller et al., 2015). Several studies in northeast South Africa have identified and discussed the importance of mixed bedrock – alluvial reaches in terms of flood response (e.g. Heritage et al., 2001a, 2001b, 2003, 2015, 2019; Knight, 2022; Knight & Evans, 2017, 2018, 2022; Maswanganye et al., 2022; Milan, 2018a, 2018b, 2020). In mixed bedrock – alluvial reaches, flood events often cause sediments to be transported from bedrock hollow to hollow (e.g. Jansen & Brierley, 2004), leading to a sediment transport system in which transport is episodic between these sites of sediment deposition and storage (Heritage et al., 2014; Milan et al., 2018a, 2018b, 2020; Rowntree et al., 2000). However, flood-transport processes and dynamics are not well known, in part because of their short-term occurrence and difficulties of *in situ* measurement and monitoring, and because the sedimentary products are difficult to interpret. However, the sedimentary stratigraphic and dating record of flood events can provide insight into the nature of sediment transport in mixed bedrock – alluvial rivers (Colarossi et al., 2015; Cunningham et al., 2015; Knight & Evans, 2017, 2018). Further work on this type of evidence can inform on river system responses to flooding in semiarid areas, especially in mixed bedrock – alluvial rivers where these responses may vary between bedrock and sedimentary substrates. In addition, to evaluate the timing of sediment deposition, luminescence dating can be applied in areas where sediments have accumulated, and this may be geologically controlled according to sites of deposition within bedrock hollows.

The aim of this study is to examine the sediment dynamics of bedrock-controlled river reaches in headwater areas of the Letaba River in northeast South Africa. This is achieved through combining field-based geomorphology, sedimentology, and dating. In particular, new luminescence ages are presented that can inform on the degree and nature of sediment reworking between bedrock-controlled sediment storage areas.

2. Study area

The Letaba River is one of several parallel-aligned river systems flowing eastwards from headwater areas along the Eastern Escarpment of South Africa, through the Kruger National Park (KNP) and into the Limpopo River system, draining into the Indian Ocean (Figure 1). The Letaba River itself has a drainage basin area of ~ 13

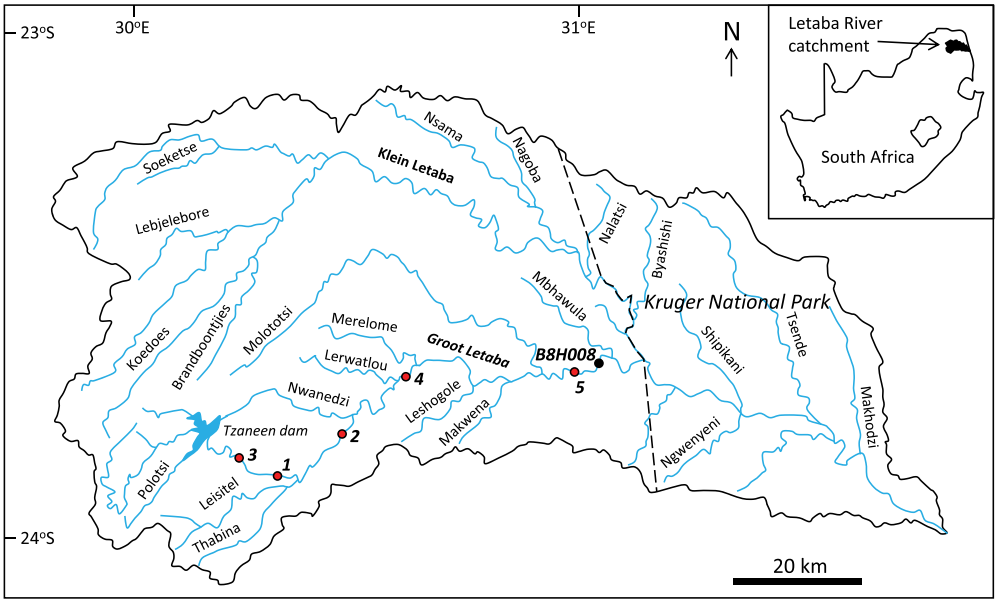


Figure 1. Location of the Letaba River catchment in northeast South Africa, the location of the five sites examined in this study (marked 1–5), and the river gauging station B8H008.

670 km^2 (State of the Rivers Report, 2001) and comprises two major tributaries: the Klein Letaba to the north and Groot Letaba to the south. Mean annual precipitation within the Letaba catchment is 622 mm but this varies substantially with 425–2000 mm yr^{-1} in the highest western headwater areas (ecoregion 2.15) of the Letaba basin, to 250–725 mm yr^{-1} in eastern lowland reaches within KNP (ecoregion 5.02) (State of the Rivers Report, 2001). In more detail, the Groot Letaba catchment's annual precipitation ranges from 1500 mm in headwater regions (<2121 m asl) in the Eastern Escarpment, to 450 mm in eastern lowland areas (155 m asl) (Graham et al., 2022). Rainfall in the region is also strongly seasonal with summer cyclonic precipitation between October and March often resulting in extreme flood events that have the capacity to lead to significant and very rapid geomorphic change (Heritage et al., 2001a, 2001b, 2014, 2019). Bedrock geology within the catchment is dominated by gneiss and granite (Schutte, 1986) and macroscale fracture patterns in these rocks influence the detailed geomorphology of pools, riffles, and rock outcrops within the river system. Bedrock geology in turn also influences soils and vegetation within the catchment (e.g. Venter, 1986). River discharge at monitoring station B8H008 at Letaba Ranch near the exit of the Groot Letaba tributary for the period 2006–15 (including the sampling period of this study which was in June 2013) is shown in Figure 2. The summer period (months DJF for 2011–12) immediately before sampling took place for this study experienced exceptionally low flow conditions, whereas the previous summers experienced total monthly flows of up to 70 million m^3 s^{-1} with concomitant potential for high river sediment transport.

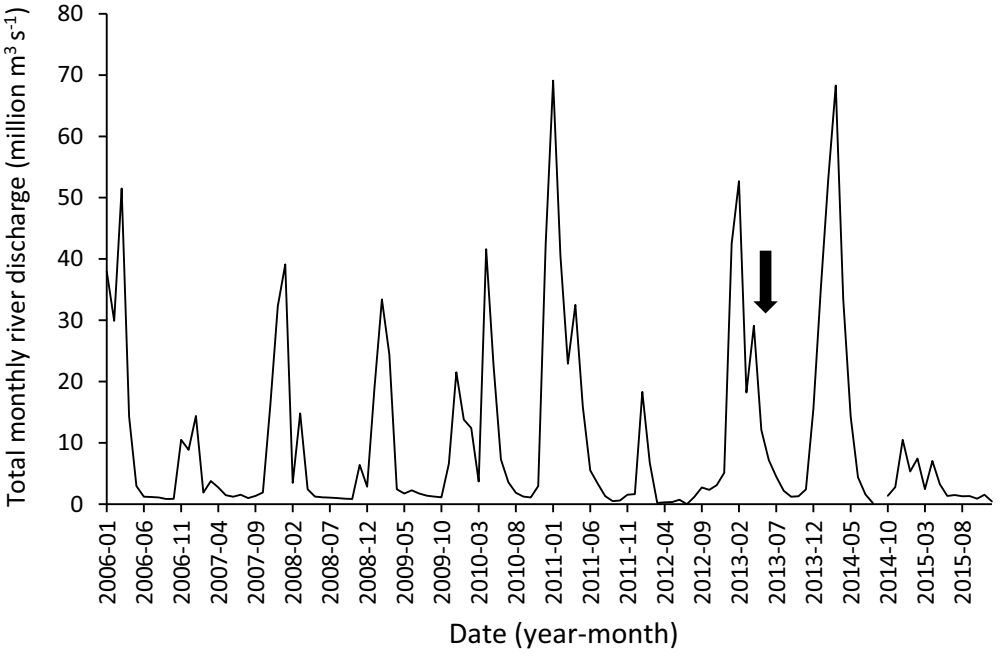


Figure 2. Total monthly river discharge volumes along the Groot Letaba, recorded at Letaba Ranch (gauge B8H008, Figure 1). The arrow indicates the sampling period in this study.

3. Methods

This study is based on a combined methodology of field observations, subsequent sediment sample analysis, and luminescence dating of sediment samples. Five sites were examined in the field, along the main river channel of the Groot Letaba located upstream of the Groot/Klein Letaba confluence and thus outside of Kruger National Park (Figure 1). Therefore, these sites correspond to headwater areas of the river where channel gradients are steeper than those found in downstream areas (Rowntree & Wadeson, 1999). The five sites were chosen pragmatically, based on their accessibility (the river flows through privately-owned property where access is restricted), fairly equidistant, and sufficiently downstream of the Tzaneen dam (constructed 1976) to reduce the impacts of artificial water release. The most upstream site, site 3, is 15 km downstream of the dam outflow. The sites also capture a range of river reach types as classified by Moon and Heritage (2001) for lower reaches of the Letaba, namely: alluvial single-thread, alluvial braided, mixed anastomosing, and mixed pool-rapid. The definitions of these reach types as described in the literature are given in Table 1. Although this classification scheme has been updated based on the River Styles Framework (Brierley et al., 2011; Fryirs & Brierley, 2018) and applied to other rivers in northeast South Africa (Eze & Knight, 2018; Knight, 2022), this previous classification is applied here to facilitate comparison between different reaches of the Letaba.

The Groot Letaba extending from the Tzaneen dam to the Groot/Klein Letaba confluence (Figure 1) was classified for reach types using historic Google Earth imagery of the same date as field data collection for this study (June 2013), in 1-km length

Table 1. River reach types identified in this study, and their definitions (adapted after Moon & Heritage, 2001).

Reach morphological type	Definition
Alluvial single thread	These are found in particular during low flow periods and correspond to situations where water is confined to a single river channel, developed on a sandy floodplain or sand sheet where no bedrock outcrops are present. Channel morphology (width, depth, sinuosity) is controlled by variations in water velocity. Outside of the active channel there may be dry and abandoned channels on the sand surface that may be activated with an increase in river discharge and therefore widening of the active channel.
Alluvial braided	Multiple distributary channels are present over a low-relief alluvial sand sheet surface. Channel number and geometry change significantly in a downstream direction with channels splitting and merging in response to changes in flow rather than being caused by any change in substrate type or the presence of any obstructions. Water discharges are similar between all channels. Outside of the active channel zone, fine grained flood deposits, small terrace-like features, abandoned sand bars and dried up ponds may be present.
Mixed anastomosing	Both bedrock and sedimentary features are found within and adjacent to the active channel. Alluvial deposits may form a thin veneer over the bedrock surface. Water may be directed into several smaller channels that split and merge, commonly controlled by the position of bedrock outcrops. Sediment may be present discontinuously as a thin sheet within the active channels. Water height and velocity may vary between different channels.
Mixed pool-rapid	Bedrock exposures dominate the active channel zone and water is confined within bedrock channels. This means that channel width/depth and planform patterns are geologically controlled, giving rise to pool–riffle structures. Pools may be floored by water-worn gravels or sand patches. Sand may be present within bedrock hollows immediately outside of the active channel zone but in all instances bedrock is the dominant control on channel morphology.

increments through the river system, which is consistent with the methodology used in previous studies (e.g. Eze & Knight, 2018; Heritage et al., 2001b; Knight, 2022; Moon & Heritage, 2001). The number of 1-km-length increments of each of the four river reach types was then calculated. It should be noted that this methodology, following that undertaken in these previous studies, examines the morphological characteristics of each 1-km long reach as a whole. At any one place along this reach, however, the precise reach type observed may be different to or more complex than what is observed at the larger scale. This is particularly important when comparing reach-scale classification (km-scale) with what may be seen in the field (m-scale).

In the field, site geomorphology was examined through observation and measurement of landforms in and around the active channel zone. Bulk surface sediment samples for characterizing the sediment population were taken from different landforms and in locations both within and away from the channel. The positions of landforms and sediment samples were obtained using a handheld GPS (horizontal accuracy of ±3 m) and differential GPS (horizontal and vertical accuracy of ±3 cm). Sediment samples from each site were analysed in the lab for grain size distributions using 0.25 ϕ sieves between 63 and 2000 μm. Calculation of derived parameters (median grain size, skewness, kurtosis) was then undertaken using the GRADISTAT program (Blott & Pye, 2001) and the Folk & Ward (1957) sediment classification scheme.

Thirteen samples were collected from the five sites for optically stimulated luminescence (OSL) dating. The locations chosen for sample collection in the field were based on the availability of suitable sediment deposits and their accessibility. Near-surface sediment (within ~10 cm of the surface) was collected preferentially as this was assumed to be the most recently deposited. Where possible, multiple samples were collected at each site, either

within the river channel or from deposits on the adjacent banks and floodplain, to constrain the ages of the different features or landforms present. The samples were collected in light-safe tubes by pushing or hammering the tubes into the sediment unit before sealing it to ensure no exposure to sunlight. Where samples were collected below the water surface, the tube was pushed into the sediment horizontally and sealed at either end before being extracted and taped securely. The sampling methodology closely follows that of Cunningham et al. (2015). In the laboratory, each sample was divided into two parts for equivalent dose (D_e) and dosimetry (D_r) measurements under safe-light conditions. Quartz grains were extracted from the D_e portion following standard OSL sample preparation protocols (see Aitken, 1997, 2014; Mahan et al., 2023). Organic matter and carbonates were removed using H_2O_2 and HCl, respectively, before the 180–212 μm quartz fraction was isolated by dry sieving and density separation using a solution of sodium polytungstate (SPT) at 2.70 g cm^{-3} and 2.63 g cm^{-3}. The alpha contribution to the dosimetry, along with any remaining feldspars, was removed by etching the quartz grains in HF for 40 minutes, following which an HCl wash was used to remove any acid-soluble fluorides.

The equivalent dose for each sample was measured using Risø TL/OSL DA-15 and DA-20 readers, in which optical stimulation was provided by blue LEDs (478 nm) of ~40 mW cm^{-2} constrained by a long-pass filter (GG-420). The OSL signal was detected with an EMI 9235QB photomultiplier tube via a single 7.5 mm Hoya U340 detection filter. The D_e values were derived by calibrating the optical signal acquired naturally during burial to the regenerated optical signals obtained through controlled laboratory doses, using the single aliquot regenerative (SAR) protocol of Murray and Wintle (2000). The suitability of the SAR protocol for determining D_e was evaluated using a combined preheat and dose recovery test, and the recycling ratio. The temperature at which a known dose was recovered within unity was selected for further measurements. The preheat also assessed the consistency of D_e as the temperature varied (Murray & Wintle, 2003). In addition, any aliquots where the recycling ratio was not within unity (between 0.9–1.1) were rejected. The D_e distributions were plotted as abanico plots following the method described by Dietze et al. (2016) and Burow et al. (2016). This approach has been used for analysing luminescence dates from several fluvial environments (Guo et al., 2023; Knight & Evans, 2018; Li et al., 2021).

For dosimetry calculations (D_r), the radionuclide abundances of U and Th were determined using ICP-MS, and K was determined using XRF. Adjustments were made to account for water content, and cosmic dose contributions were determined following the method outlined by Prescott and Hutton (1994). Dose rate conversion followed the approach by Guérin et al. (2011), and the age was calculated by dividing D_e by D_r, following procedures described in Aitken (1985) (see also Mahan et al., 2023). All error terms provided are computed at one sigma level.

4. Results

4.1. Geomorphic and sedimentary characterization of river reaches

In total, 161 km of river length was measured and classified for reach type between the Tzaneen dam and the Groot/Klein Letaba confluence. Of these 161 × 1 km-long segments, mixed anastomosing is most common (59, 37%), followed by alluvial single thread channels

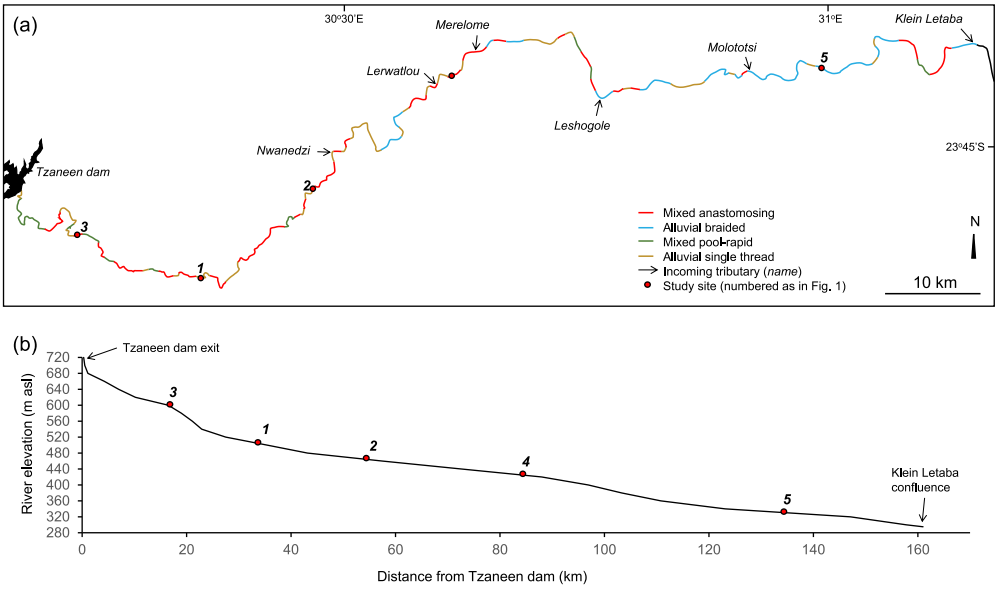


Figure 3. (a) River reach classification at 1-km intervals (see definitions in Table 1), using the scheme of Moon & Heritage (2001), for the groot letaba between Tzaneen dam and the Klein/Groot Letaba confluence. Study sites and the position of major tributaries are marked. (b) River long profile along the groot letaba showing the position of the study sites, based on contours (at 20 m intervals) shown on 1:50 000-scale maps for this area.

(42, 26%), alluvial braided (41, 25%), and then mixed pool-rapid (19, 12%) (Figure 3(a)). The presence of both bedrock and surface sediments in different proportions, therefore, characterizes the Groot Letaba. Mixed pool-rapid reaches are found mainly in steeper headwater areas whereas in a downstream direction surface sediment becomes more common as the river's long profile becomes less steep and river valleys wider (Figure 3 (b)). It is notable that the Groot/Klein Letaba confluence has an alluvial braided channel which also continues 4 km downstream according to the reach classification mapping undertaken by Heritage et al. (2001, their Figure 2(a)). The geomorphic context and relative positions of the OSL dating samples to the active river channel(s) at each site are shown in Figure 4. The detailed geomorphology and sediment properties at the five sample sites are now described from Site 3, which is the most upstream site, in a downstream direction towards the confluence of the Groot/Klein Letaba.

Site 3 (23°50'37.2"S, 30°13'02.8"E) is located on a mixed anastomosing reach adjacent to a bridge at Fleurbaai near Letaba River Lodge (Figure 5). The reach is dominated by bedrock ridges and hollows that split the low-flow river into different anastomosing and braided channels that are located at different elevations. These landforms are present across the total width of the river valley (60 m), but the presence of trees and shrubs set between abandoned channels shows that different parts of the river system were active at different times, caused by changes in water height (and therefore discharge) during floods (Figure 5(c)). Flood debris including tree branches is present up to 1.5 m above the present water level. Near to the present active channel, the relative relief of the bedrock ridges is some <1.6 m above water level. Bedrock fractures (aligned at 080–260°

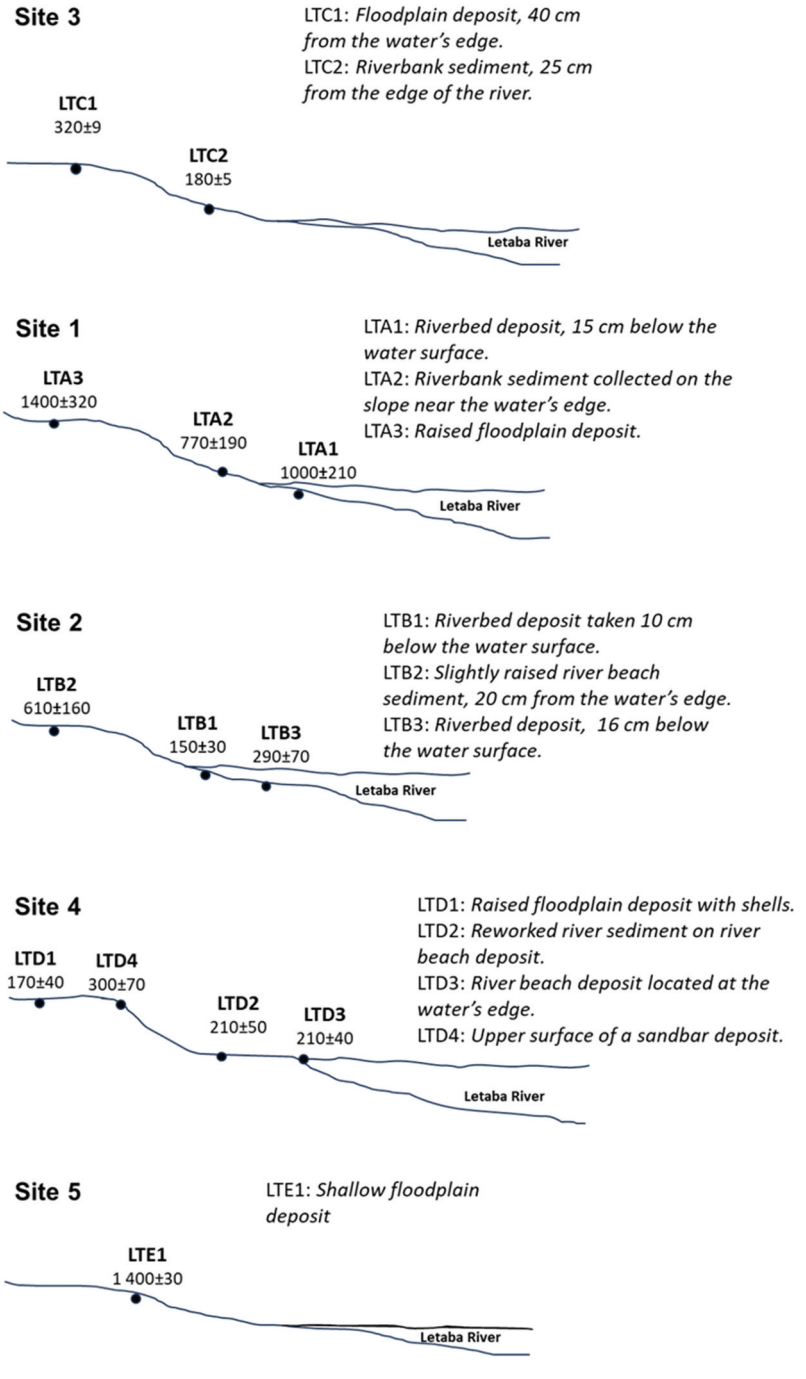


Figure 4. Field sketches showing the locations of OSL dating samples relative to the Letaba River, for each site (Figure 3). Note the field sketches are for illustrative purposes only and are not to a measured scale. Information regarding each sample is provided and the details of the luminescence ages are given in Table 3.



Figure 5. Photos of site properties and landforms from site 3. (a) Mixed bedrock and alluvial main channel, (b) potholes developed in bedrock above the observed water surface and suggestive of turbulent flow during flood stages, (c) well-developed riparian vegetation stabilizing channel banks, (d) bedrock pool and gravel accumulation within the channel, (e) meander bend, where bedrock controls on channel morphology decreases, (f) sculpted bedrock channel forms typical of high-energy floodwater.

and 100–280°) have influenced the geometry of bedrock ridges where these lines of weakness have been exploited by hydraulic action and abrasion (Figure 5(b)). Plucking of individual fracture-defined boulders leaves a socket (15–25 cm diameter) into which sediment can be deposited. Rounded, abraded potholes with boulders at their base are also present. Individual bedrock channels and pools are 1.5–6 m wide and <1 m deep. Throughout, bedrock surfaces are smoothed and polished; occasionally, isolated detached boulders are present on elevated rock surfaces or within the channel. Located

within bedrock hollows <1.5 m above the water-filled channel are patches of poorly sorted granules to boulders. A sediment sample from one of these patches (sample 3–2, Table 2) yields moderately sorted coarse sand which is coarser than sediments within a subaqueous bar in the largest and deepest channel (sample 3–1).

Site 1 (23°52'49.0"S, 30°21'02.9"E) is located in an alluvial single thread reach near the informal settlement of Mariveni where the river was approximately 30 m wide and 1 m deep at the time of sampling and where river sand is being mined by hand by informal miners. Here, the single river channel is set in a floodplain context with river banks 1.1–1.8 m high and composed of medium to coarse fluvial sand layers (Figure 6(b)). Outside of the immediate channel banks is a terrace 4 m above the present river level. A sand sample (sample 1–1, Table 2) from the terrace surface shows poorly sorted medium sand. A sample from the base of the terrace, 50 cm above the active channel, is composed of poorly sorted coarse sand (sample 1–2).

Site 2 (23°47'21.8"S, 30°28'07.3"E) is located on a mixed anastomosing reach between Nagude and Riverside. Bedrock outcrops and detached boulders are present throughout and across the extensive floodplain (60 m wide, separated by a vegetated bedrock mid-channel island). Boulders (<90 cm diameter) are commonly stacked and imbricated within and around the main channel and may show chattermarks indicative of attrition during transport. Outside of the present channel, bedrock surfaces are of low relief with a scatter of pebbles either in bedrock hollows or as an armour across a coarse sand and granule plain surface (Figure 7(a–c)). A sand sample from this outer channel plain (sample 2–1, Table 2) shows moderately sorted coarse sand. Relict sand bars are also observed in places across the floodplain, with a pebble armour and a sandy tail. A sediment sample from this bar tail (sample 2–2) shows moderately sorted medium sand. Flood debris caught in tree branches is located 2 m above the present water surface.

Site 4 (23°41'02.2"S, 30°36'34.4"E) is located on a mixed anastomosing reach adjacent to a bridge at Letaba Drift. A single river channel is present alongside an extensive floodplain (20 m width) comprised of bedrock outcrops and sandbanks. Bedrock is laterally extensive adjacent to the main river channel, with broken and abraded bedrock surfaces, detached bedrock boulders and isolated pockets of transported gravel (Figure 8(a,b)). The large sand banks (<2 m high), located outside of activity in the main channel and adjacent to the floodplain margin, comprise poorly sorted very coarse sand with freshwater mollusc shells forming a horizontal 'watermark' across the bank surface typical of a descending water surface (Figure 8(c)). The elongated sandbanks coarsen in a downflow direction and have scour channels around their margins (Figure 8(d)). Internally, the sand banks also show cm-scale normally-graded planar bedding. Dune bedforms are also superimposed upon each other; sediment samples from one such situation show moderately well-sorted coarse sand (sample 4–2) superimposed upon an earlier moderately sorted medium sand dune (sample 4–3). Sand bodies associated with flooding from the main channel form relatively flat terraces 12 m wide and <1 m above the present water surface. A sediment sample from this elevated surface (sample 4–1, Table 2) comprises very well-sorted medium sand, typical of active sediment transport. Flood debris is found within tree branches at 5 m elevation above the ground surface and 6.5 m above the present water surface.

Site 5 (23°40'16.4"S, 30°59'24.9"E) is located on an alluvial braided reach within Hans Merensky Nature Reserve at La Cotte. Here, the river channel has incised into the

Table 2. Letaba River sediment sample properties from upstream to downstream sites. Locations of sites are shown in Figure 1. Sites are shaded in the table merely to assist the reader.

Site/sample	Sample location	Sample D_{10} value (μm)	Sample D_{50} value (μm)	Sample D_{90} value (μm)	Sediment sample description	Sorting	Skewness	Kurtosis
3–1	End of mid channel bar within the active channel	247	518	1051	Slightly gravelly coarse sand	Moderately sorted	Symmetric	Mesokurtic
3–2	Sand patch on a bedrock surface above the present channel	467	831	1473	Slightly gravelly coarse sand	Moderately sorted	Symmetric	Mesokurtic
1–1	4 m terrace	136	415	1119	Slightly gravelly medium sand	Poorly sorted	Symmetric	Mesokurtic
1–2	Base of terrace, 50 cm above the active channel	215	512	1285	Slightly gravelly coarse sand	Poorly sorted	Symmetric	Mesokurtic
2–1	Sand plain outside the active channel	314	715	1393	Slightly gravelly coarse sand	Moderately sorted	Fine skewed	Mesokurtic
2–2	Sand bar tail	232	422	671	Slightly gravelly medium sand	Moderately well sorted	Fine skewed	Mesokurtic
4–1	Sand terrace located above the present channel	363	457	565	Slightly gravelly medium sand	Very well sorted	Symmetric	Leptokurtic
4–2	Relict sand bank	365	661	1156	Slightly gravelly coarse sand	Moderately well sorted	Symmetric	Mesokurtic
4–3	Relict sand bank	186	379	674	Slightly gravelly medium sand	Moderately sorted	Symmetric	Mesokurtic
5–1	River channel sides	118	353	875	Slightly gravelly medium sand	Poorly sorted	Symmetric	Mesokurtic

Table 3. Luminescence ages from the samples used in this study. Calculated ages in the final column refer to years before the sampling period (2013). Sites are shaded in the table merely to assist the reader. The relative positions of the samples at each site are shown in Figure 4.

Site number (Figure 1)	Lat Long	Sample location (Figure 4)	Lab code	Altitude (m asl)	Sample depth (m)	Water content (%)	Th (ppm)	U (ppm)	K (%)	D_r (Gy ka^{-1})	Overdispersion (%)	D_e (CAM) (Gy)	CAM age (ka)	Calculated age (yr BP)
3	23°50′37.2″S, 30°13′02.8″E	River bank, 40 cm from water's edge	LTC1	608	0.01	5 ± 2	7.75	1.215	1.8	2.38 ± 0.07	1.01 ± 0.05	0.77 ± 0.21	0.32 ± 0.09	320 ± 90
		River bank, 25 cm from water's edge	LTC2	608	0.01	5 ± 2	7.75	1.215	1.8	2.38 ± 0.07	1.1 ± 0.04	0.44 ± 0.11	0.18 ± 0.05	180 ± 50
1	23°52′49.0″S, 30°21′02.9″E	15 cm below water surface	LTA1	550	0.15	5 ± 2	7.75	1.215	1.8	2.65 ± 0.08	1.01 ± 0.03	2.67 ± 0.55	1.00 ± 0.21	1000 ± 210
		River bank at water's edge	LTA2	550	0.01	5 ± 2	7.75	1.215	1.8	2.38 ± 0.07	1.10 ± 0.04	1.83 ± 0.44	0.77 ± 0.19	770 ± 190
		Floodplain deposit	LTA3	550	0.01	5 ± 2	7.75	1.215	1.8	2.38 ± 0.07	1.10 ± 0.03	3.33 ± 0.76	1.40 ± 0.32	1400 ± 320
2	23°47′21.8″S, 30°28′07.3″E	In river 10 cm below water surface	LTB1	635	0.10	5 ± 2	7.75	1.215	1.8	2.60 ± 0.08	0.85 ± 0.03	0.40 ± 0.08	0.15 ± 0.03	150 ± 30
		Slightly raised river beach, 20 cm from water's edge	LTB2	635	0.20	5 ± 2	7.75	1.215	1.8	2.69 ± 0.08	0.90 ± 0.05	1.63 ± 0.42	0.61 ± 0.16	610 ± 160
		In river, 16 cm below water surface	LTB3	635	0.16	5 ± 2	7.75	1.215	1.8	2.67 ± 0.08	0.84 ± 0.05	0.76 ± 0.19	0.29 ± 0.07	290 ± 70
4	23°41′02.2″S, 30°36′34.4″E	Raised flood deposit	LTD1	417	0.01	5 ± 2	7.75	1.215	1.8	2.37 ± 0.07	1.00 ± 0.04	0.39 ± 0.09	0.17 ± 0.04	170 ± 40
		Reworked sediment below flood deposit	LTD2	417	0.01	5 ± 2	7.75	1.215	1.8	2.37 ± 0.07	1.1 ± 0.04	0.51 ± 0.13	0.21 ± 0.05	210 ± 50
		On water's edge	LTD3	417	0.01	5 ± 2	7.75	1.215	1.8	2.37 ± 0.07	0.60 ± 0.05	0.49 ± 0.10	0.21 ± 0.04	210 ± 40
		Upper surface of fine bar deposit between LTD1 and LTD2	LTD4	417	0.01	5 ± 2	7.75	1.215	1.8	2.37 ± 0.07	1.1 ± 0.04	0.71 ± 0.17	0.30 ± 0.07	300 ± 70
5	23°40′16.4″S, 30°59′24.9″E	Floodplain deposit	LTE1	271	0.15	5 ± 2	7.75	1.215	1.8	2.64 ± 0.08	0.94 ± 0.03	3.68 ± 0.78	1.40 ± 0.30	1400 ± 300



Figure 6. Photos of site properties and landforms from site 1. (a) View downstream, where the river banks are stabilized by vegetation, (b) sediments shown within the river channel (the brown water colour) and within the river banks.

adjacent floodplain where planar bedded sands and silts with lenses of granules are exposed (Figure 9). A sediment sample from the present channel (sample 5–1, Table 2), presumably reworked from the eroded channel bank, shows poorly sorted medium sand.

4.2. Dating evidence

The luminescence ages obtained in this study are presented in Table 3. The ages range from the youngest sample of 150 ± 30 years at LTB1 (site 2) to the oldest of 1400 ± 320 years at LTA3 (site 1) and LTE1 (site 5). All the samples have an overdispersion greater than 20%, suggesting scatter within the dataset that cannot be ascribed to instrumental error alone. The scatter in the D_e distribution is also displayed in abanico plots (Figure 10). The scatter can be attributed to the reworking of the sediment during flood events resulting in incomplete bleaching of the luminescence signal in the flood-transported grains (Cunningham et al., 2015; Mahan et al., 2023). Even the sample with the lowest overdispersion (LTD3), taken at the



Figure 7. Photos of site properties and landforms from site 2. (a) Gravel dominated river channel with outsized boulders within the channel itself, (b) scatter of flood-deposited imbricated boulders located outside of the main channel, (c) variations in water velocity within the main channel as a result of differences in channel depth caused by the distribution of boulders, (d) boulder scatters paving the bed of a broad and shallow channel.

water's edge, has not been fully exposed to sunlight to reset the previous signal. Where the overdispersion is greater than 20%, the minimum age model (MAM) is reported (Galbraith et al., 1999). However, negative D_e values were recorded (although not included in the age calculation), suggesting that some grains were exposed to sunlight just prior to sampling, indicating a present-day age. Therefore, the MAM would not be meaningful in this instance and so dates were calculated and reported using the central age model (CAM) (Galbraith et al., 1999). The ages are given as years before the date of sampling (2013). The spread of ages obtained are presented graphically in Figure 11.

5. Discussion

Floods are a well-known geomorphic agent in the semiarid rivers of northeast South Africa (Rountree et al., 2000; Heritage et al., 2001a, 2001b, 2003). As such, it should be anticipated that a range of geomorphic and sedimentary evidence for past recent floods would be found in these systems. The wide and dominantly mixed bedrock – alluvial floodplains found in headwater regions of the Letaba River are most commonly of mixed anastomosing type where both bedrock and sediment surfaces are present (Figure 3). These different substrate types are affected by floodwaters in different ways according to



Figure 8. Photos of site properties and landforms from site 4. (a) Bedrock dominated single channel with boulder scatters on the areas outside of the active channel, (b) eroded bedrock with hollows containing flood-transported cobbles and other debris, (c) poorly sorted sediment bank alongside the active channel indicative of sediment transport and deposition during higher flow stages, (d) cobble-filled relict channel, landward of a sediment bank or flood bar, that would have been active during higher flow stages.



Figure 9. Photo of sediment stratigraphy within the river bank at site 5.

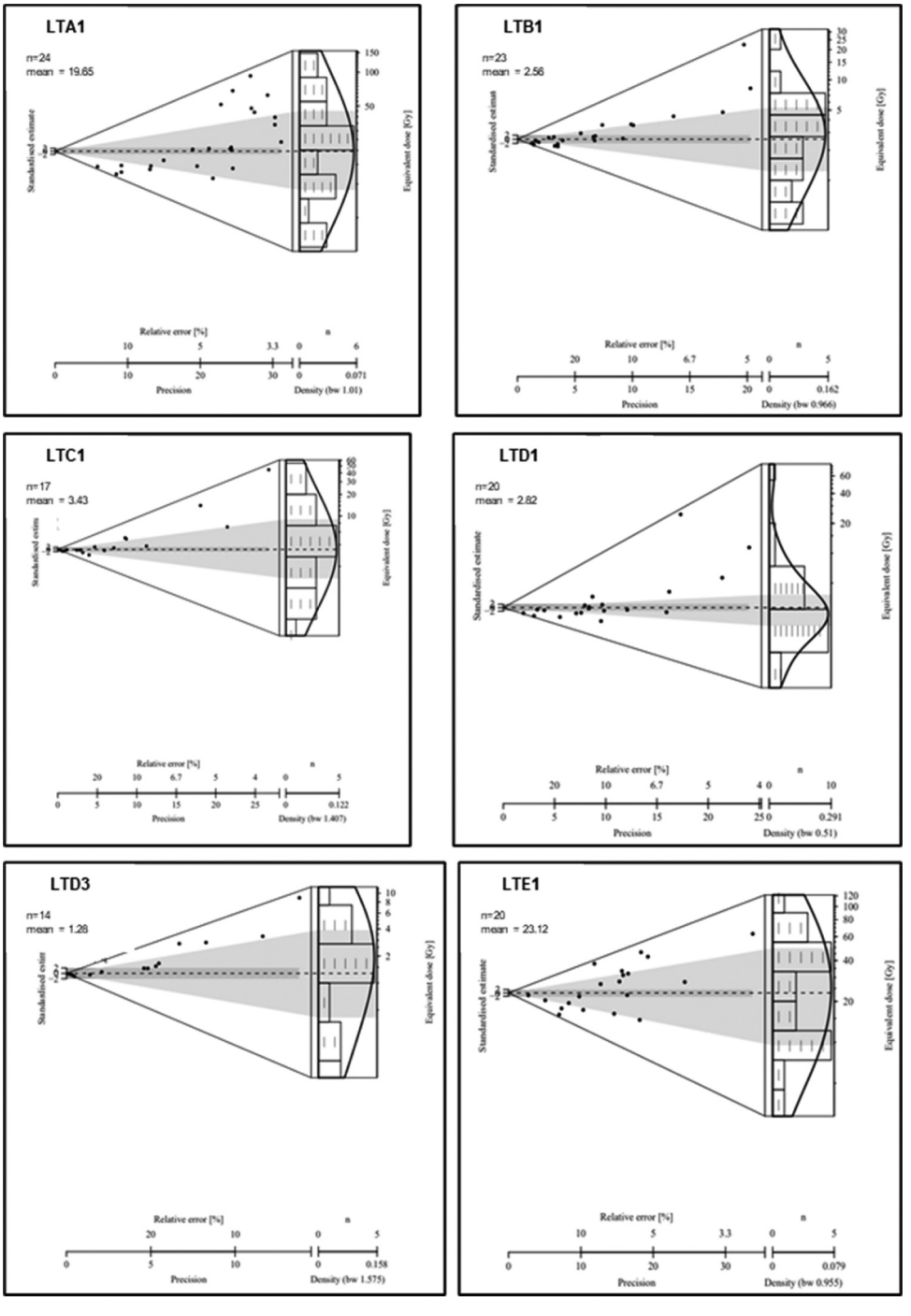


Figure 10. Examples of abanico plots showing the D_e distribution of samples. The distribution is centred around the central age model (CAM) (shaded area). LTD3 shows the distribution with the lowest overdispersion (greatest clustering).

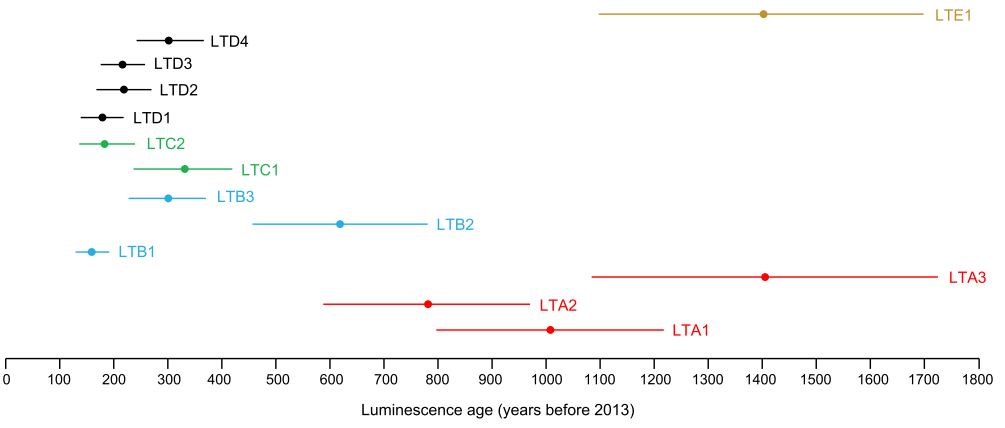


Figure 11. Plot of CAM ages with errors for the luminescence samples in this study (Table 3). Samples from the same sites are colour-coded to aid comparison. LTA = site 1, LTB = site 2, LTC = site 3, LTD = site 4, LTE = site 5.

bed roughness, variations in water height and velocity (which vary across the floodplain due to its surface elevation and landforms) (Heritage et al., 2003), and through feedback associated with patterns of sediment erosion *versus* deposition during the flood cycle (Knight & Evans, 2022). The coarse and poorly sorted sediments found throughout the system (Table 2) reflect high water velocities and rapid deposition, forced when water ponds across the wide floodplain after the initial flood wave (Knight & Evans, 2017). The sediment and loose boulder accumulations are mainly found within bedrock hollows but, as shown at site 4, elongate mobile dune forms are also found, located outside of the low-flow channel, and thus formed by saltation during maximal flood conditions (Figure 8(c, d)). If sediments are mobilized by water at different flood stages (i.e. water heights), then it is likely that sediments and bedforms at higher elevations are active for shorter periods of time, being quickly stabilized as water level and water velocity decline, whereas sediments in the low-flow channel remain active for longer periods.

The luminescence dates obtained in this study (Table 3) broadly cluster around three time periods: the last 400 years (eight dates, sites 2–4), 500–1100 BP (three dates, site 1, 2), and around 1400 BP (two dates, sites 1, 5) (Figure 11). The sites where these date ranges are found may broadly reflect their large-scale geomorphology. The youngest ages are found at mixed anastomosing sites that have a relatively broad floodplain with low elevation bedrock hollows where sediments can accumulate, and from which sediments can be rapidly reworked when the water surface rises during floods (Heritage et al., 2003). This is also confirmed by their relatively narrow age errors, indicative of signal zeroing during transport (Cunningham et al., 2015). Samples of intermediate age (LTA2, LTB2) are found at slightly higher elevations and outside of the main active channel zone. The oldest ages are associated with alluvial environments where the dated sediments have likely been reworked from terrace stratigraphies formed by overbank deposition during floods, as evidenced by the thick alluvial sequences seen at these sites (Figures 6, 9). It is notable that under such conditions, sediments are commonly poorly bleached within the water column, resulting in higher age error ranges (Knight & Evans, 2018). Overall, the relatively young ages in this study, within the last millennium, are consistent with luminescence ages from other South African rivers (Figure 12), also interpreted as flood-influenced.

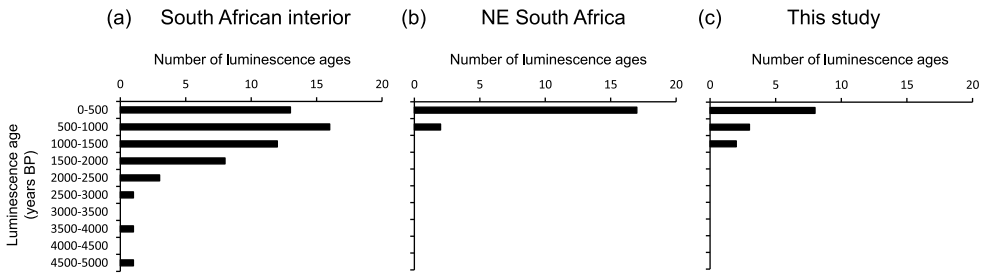


Figure 12. Comparison of the distribution of late holocene luminescence ages (last 5000 years) obtained from river deposits in South Africa. Dates from (a) rivers in the the South African interior (Keen-Zebert et al., 2013; Larkin et al., 2017; Tooth et al., 2007), (b) the Sabie River in semiarid northeast South Africa (Heritage et al., 2014; Knight & Evans, 2018), and (c) the upper Letaba River in this study (Table 3).

It is notable that luminescence ages from sandy rivers in the South African interior such as the Tshwane, Klip and Mooi are significantly older, mainly because these dates are from low-gradient reaches where avulsion and meander abandonment are common. Pre-Holocene ages are also recorded from these rivers. By contrast, dates from the semiarid Sabie River (Figure 12 (b)) are on the order of decades to hundreds of years, but significantly younger than those recorded for the Letaba in this study. However, the Sabie dates are all from lowland alluvial reaches of the river within KNP, where river discharge is higher and where floods may be considered as more likely and sediments more commonly reworked, whereas the Letaba dates are from headwater reaches farther inland that may have different rainfall event and sediment reworking histories (Saraiva Okello et al., 2015). It is these headwater reaches that have not been considered in detail previously.

River flood events are associated with a low capacity for sediment luminescence bleaching and age-zeroing during transport, due to the short time over which sediments are in transport, and the high density of particles in the water column (Gray & Mahan, 2015; Jain et al., 2004). This means that dated samples are only partially bleached, as shown by the distribution of D_e values on the abanico plots (Figure 10) and the high overdispersion (Table 3), and thus retain the residual signals indicative of their previous depositional and transport histories (Cunningham et al., 2015). This results in both a greater age error (Table 3) and a larger scatter of equivalent dose (D_e) values (Figure 11). Although these ages from single sediment layers themselves cannot be used to identify the timing of past flood events, they indicate the sensitivity of river systems to be affected by flood events brought about through climate/weather forcing, in which sediments are progressively and episodically reworked through the river system.

The geomorphological sensitivity of river systems reflects both the nature of climate forcing through high rainfall events, and catchment properties such as slope, vegetation, substrate type and human activity that can modify river system geomorphic and sedimentary responses (Brunsden & Thornes, 1979; Buraas et al., 2014; Downs & Gregory, 1995). Episodic flood events are associated with periods of rapid geomorphic change (Milan et al., 2018a; Rountree et al., 2000) where critical thresholds of sediment transport are exceeded. This is often followed by periods of more subdued sediment transport activity and where sediments may be reworked around the active channel rather than on more distal parts of the floodplain (Fryirs et al., 2012; Knight & Evans, 2017, 2022; Rountree et al., 2000). Previous work on

sediment systems within rivers tends to consider a single river reach as a uniform sediment storage site (e.g. Fryirs et al., 2007) but, in reality, the dynamics of river sediment transport also vary laterally across the floodplain (with distance from the low-flow channel as well as in response to variations in bedrock versus sediment substrates) (Fryirs, 2013; Knight & Evans, 2018). This means that the geomorphological sensitivity of river systems will vary spatially (from one reach to another, with distance from the active channel) and temporally where bedrock surfaces are revealed/covered by sediment erosion and deposition, respectively. This property of changing geomorphological sensitivity, along with site-specific controls such as grain size and elevation above the low-flow channel, may help explain the range of ages obtained from the headwater system (Table 3). Here, this may suggest that the mixed anastomosing channels and the presence of bedrock depositional hollows at different elevations (e.g. Figures 5–8) allow for preferential preservation of sand bodies, favouring older dates. Floods of different elevations or magnitudes may be able to rework or remove certain sand bodies but leave others intact. Therefore, floods are not able to uniformly 'reset' the river system as argued in previous studies (e.g. Heritage et al., 2003, 2014), but rather their impacts are conditioned by, and in turn, can influence, the sensitivity of the river system within which they operate. This is a more nuanced framework for understanding the role of floods on semiarid rivers.

6. Conclusions

This study shows that the headwater areas of the semiarid Groot Letaba River, northeast South Africa, have a varied but mixed geomorphology that exhibits different sensitivities to forcing by flood events. Evidence for this comes from spatial patterns and properties of sediments and landforms within individual reaches, and variations in reach geomorphology through the river system. New luminescence ages confirm the episodic nature of sediment reworking by floods; however, the nature of sediment transport fluxes between successive bedrock depocentres is not well understood, which means that the timescales over which sediment is captured within depocentres or is reworked between them is also not well known. The new dates presented here highlight that some sediments are rapidly reworked (ages of a few hundred years) whereas others have greater longevity within the river system (ages over 1000 years). This is likely related to their depositional setting across the floodplain and elevation above the low-flow channel (Figure 4). It also highlights that patterns of sediment reworking and geomorphic dynamics of headwater reaches may be different to those found on lowland alluvial reaches, even along the same river. Future work may involve more detailed sampling and measurement of sediment luminescence signals along floodplain transects to identify its spatial variability. It may also include examining the geomorphology and luminescence ages of the adjacent Klein Letaba tributary, to see if there are similar sediment reworking patterns across the entire Letaba catchment.

Acknowledgments

This study was supported by National Research Foundation grant 91344 (to JK). We are very grateful to SANParks for permission to undertake research in Kruger National Park (permit KNIGJ1225) and for logistic support. We thank several anonymous reviewers for their comments on this paper.

Disclosure statement

No potential conflict of interest was reported by the author(s).

Funding

The work was supported by the NRF [91344].

ORCID

Jasper Knight http://orcid.org/0000-0003-2035-9056

References

Heritage, G. L., Moon, B. P., & Large, A. R. G. (2001a). The February 2000 floods on the Sabie River, South Africa: an examination of the magnitude and frequency. Koedoe, 44(1), 37–44. https://doi.org/10.4102/koedoe.v44i1.184.

Heritage, G. L., Moon, B. P., & Large, A. R. G. (2001b). The February 2000 floods on the Letaba River, South Africa: an examination of magnitude and frequency. Koedoe, 44(2), 1–6. https://doi.org/10.4102/koedoe.v44i2.171.

Aitken, M. J. (1985). *Thermoluminescence Dating*. London: Academic Press.

Aitken, M. J. (1997). Luminescence dating. In R. E. Taylor & M. J. Aitken (Eds.), *Chronometric Dating in Archaeology* (pp. 183–216). Berlin: Springer.

Aitken, M. J. (2014). *Science-Based Dating in Archaeology*. London: Routledge.

Baggs Sargood, M., Cohen, T. J., Thompson, C. J., & Croke, J. (2015). Hitting rock bottom: Morphological responses of bedrock-confined streams to a catastrophic flood. *Earth Surface Dynamics*, *3*(2), 265–279. https://doi.org/10.5194/esurf-3-265-2015

Baynes, E. R. C., Lague, D., Steer, P., Bonnet, S., & Illien, L. (2020). Sediment flux-driven channel geometry adjustment of bedrock and mixed gravel–bedrock rivers. *Earth Surface Processes and Landforms*, *45*(14), 3714–3731. https://doi.org/10.1002/esp.4996

Blott, S. J., & Pye, K. (2001). GRADISTAT: A grain size distribution and statistics package for the analysis of unconsolidated sediments. *Earth Surface Processes and Landforms*, *26*(11), 1237–1248. https://doi.org/10.1002/esp.261

Brierley, G., Fryirs, K., Cook, N., Outhet, D., Raine, A., Parsons, L., & Healey, M. (2011). Geomorphology in action: Linking policy with on-the-ground actions through applications of the river styles framework. *Applied Geography*, *31*(3), 1132–1143. https://doi.org/10.1016/j.apgeog.2011.03.002

Broadhurst, L. J., & Heritage, G. L. (1998). Modelling stage-discharge relationships in anastomosing bedrock-influenced sections of the Sabie River system. *Earth Surface Processes and Landforms*, *23*(5), 435–465. https://doi.org/10.1002/(SICI)1096-9837(199805)23:5<455:AID-ESP860>3.0.CO;2-2

Brunsden, D., & Thornes, J. B. (1979). Landscape sensitivity and change. *Transactions of the Institute of British Geographers NS*, *4*(4), 463–484. https://doi.org/10.2307/622210

Buraas, E. M., Renshaw, C. E., Magilligan, F. J., & Dade, W. B. (2014). Impact of reach geometry on stream channel sensitivity to extreme floods. *Earth Surface Processes and Landforms*, *39*(13), 1778–1789. https://doi.org/10.1002/esp.3562

Burow, C., Kreutzer, S., Dietze, M., Fuchs, M. C., Fischer, M., Schmidt, C., & Brückner, H. (2016). RLumShiny – a graphical user interface for the R package 'luminescence'. *Ancient TL*, *34*(2), 22–32.

Colarossi, D., Duller, G. A. T., Roberts, H. M., Tooth, S., & Lyons, R. (2015). Comparison of paired quartz OSL and feldspar post-IR IRSL dose distributions in poorly bleached fluvial sediments from South Africa. *Quaternary Geochronology*, *30*, 233–238. https://doi.org/10.1016/j.quageo.2015.02.015

Cunningham, A. C., Evans, M., & Knight, J. (2015). Quantifying bleaching for zero-age fluvial sediment: A Bayesian approach. *Radiation Measurements*, *81*, 55–61. https://doi.org/10.1016/j.radmeas.2015.04.007

Dietze, M., Kreutzer, S., Burow, C., Fuchs, M. C., Fischer, M., & Schmidt, C. (2016). The abanico plot: Visualising chronometric data with individual standard errors. *Quaternary Geochronology*, *31*, 12–18. https://doi.org/10.1016/j.quageo.2015.09.003

Downs, P. W., & Gregory, K. J. (1995). Approaches to river channel sensitivity. *The Professional Geographer*, *47*(2), 168–175. https://doi.org/10.1111/j.0033-0124.1995.168_v.x

Eze, P. N., & Knight, J. (2018). A geomorphological characterisation of river systems in South Africa: A case study of the sabie river. *Physics and Chemistry of the Earth*, *105*, 196–205. https://doi.org/10.1016/j.pce.2018.01.001

Folk, R. L., & Ward, W. C. (1957). Brazos River bar: A study in the significance of grain size parameters. *Journal of Sedimentary Petrology*, *27*(1), 3–26. https://doi.org/10.1306/74D70646-2B21-11D7-8648000102C1865D

Fryirs, K. (2013). (Dis)Connectivity in catchment sediment cascades: A fresh look at the sediment delivery problem. *Earth Surface Processes and Landforms*, *38*(1), 30–46. https://doi.org/10.1002/esp.3242

Fryirs, K. A., & Brierley, G. J. (2018). What's in a name? A naming convention for geomorphic river types using the river styles framework. *PLoS One*, *13*(9), e0201909. https://doi.org/10.1371/journal.pone.0201909

Fryirs, K., Brierley, G. J., & Erskine, W. D. (2012). Use of ergodic reasoning to reconstruct the historical range of variability and evolutionary trajectory of rivers. *Earth Surface Processes and Landforms*, *37*(7), 763–773. https://doi.org/10.1002/esp.3210

Fryirs, K. A., Brierley, G. J., Preston, N. J., & Kasai, M. (2007). Buffers, barriers and blankets: The (dis)connectivity of catchment-scale sediment cascades. *Catena*, *70*(1), 49–67. https://doi.org/10.1016/j.catena.2006.07.007

Galbraith, R. F., Roberts, R. G., Laslett, G. M., Yoshida, H., & Olley, J. M. (1999). Optical dating of single and multiple grains of quartz from jinmium rock shelter, northern Australia: Part I, experimental design and statistical models. *Archaeometry*, *41*(2), 339–364. https://doi.org/10.1111/j.1475-4754.1999.tb00987.x

Graham, L. P., Andersson, L., Warburton Toucher, M., Wikner, J. J., & Wilk, J. (2022). Seasonal local rainfall and hydrological forecasting for Limpopo communities – a pragmatic approach. *Climate Services*, *27*, 100308. https://doi.org/10.1016/j.cliser.2022.100308

Gray, H. J., & Mahan, S. A. (2015). Variables and potential models for the bleaching of luminescence signals in fluvial environments. *Quaternary International*, *362*, 42–49. https://doi.org/10.1016/j.quaint.2014.11.007

Grenfell, S. E., Grenfell, M. C., Rowntree, K. M., & Ellery, W. N. (2014). Fluvial connectivity and climate: A comparison of channel pattern and process in two climatically contrasting fluvial sedimentary systems in South Africa. *Geomorphology*, *205*, 142–154. https://doi.org/10.1016/j.geomorph.2012.05.010

Guérin, G., Mercier, N., & Adamiec, G. (2011). Dose-rate conversion factors: Update. *Ancient TL*, *29*(1), 5–8.

Guo, Y., Ge, Y., Mao, P., & Liu, T. (2023). A comprehensive analysis of holocene extraordinary flood events in the Langxian gorge of the Yarlung Tsangpo River valley. *Science of the Total Environment*, *863*, 160942. https://doi.org/10.1016/j.scitotenv.2022.160942

Heitmuller, F. T., Hudson, P. F., & Asquith, W. H. (2015). Lithologic and hydrologic controls of mixed alluvial–bedrock channels in flood-prone fluvial systems: Bankfull and macrochannels in the Llano River watershed, central Texas, USA. *Geomorphology*, *232*, 1–19. https://doi.org/10.1016/j.geomorph.2014.12.033

Heritage, G., Entwistle, N., Milan, D., & Tooth, S. (2019). Quantifying and contextualising cyclone-driven, extreme flood magnitudes in bedrock-influenced dryland rivers. *Advances in Water Resources*, *123*, 145–159. https://doi.org/10.1016/j.advwatres.2018.11.006

Heritage, G. L., Large, A. R. G., Moon, B. P., & Birkhead, A. L. (2003). Estimating extreme flood magnitude in bedrock-influenced channels using representative reach-based channel resistance data. *Geografiska Annaler*, *85A*(1), 1–11. https://doi.org/10.1111/1468-0459.00184

Heritage, G., Tooth, S., Entwistle, N., & Milan, D. (2014). Long-term flood controls on semi-arid river form: Evidence from the Sabie and Olifants rivers, eastern South Africa. *IAHS Publication*, *367*, 141–146. https://doi.org/10.5194/piahs-367-141-2015

Jain, M., Murray, A. S., & Bøtter-Jensen, L. (2004). Optically stimulated luminescence dating: How significant is incomplete light exposure in fluvial environments? *Quaternaire*, *15*(1–2), 143–157. https://doi.org/10.3406/quate.2004.1762

Jansen, J. D., & Brierley, G. J. (2004). Pool-fills: A window to palaeoflood history and response in bedrock-confined rivers. *Sedimentology*, *51*(5), 901–925. https://doi.org/10.1111/j.1365-3091.2004.00643.x

Johnson, K. N., & Finnegan, N. J. (2015). A lithologic control on active meandering in bedrock channels. *GSA Bulletin*, *127*(11–12), 1766–1776. https://doi.org/10.1130/B31184.1

Keen-Zebert, A., Tooth, S., Rodnight, H., Duller, G. A. T., Roberts, H. M., & Grenfell, M. (2013). Late Quaternary floodplain reworking and the preservation of alluvial sedimentary archives in unconfined and confined river valleys in the eastern interior of South Africa. *Geomorphology*, *185*, 54–66. https://doi.org/10.1016/j.geomorph.2012.12.004

Knight, J. (2022). Geomorphology and landscapes of the Limpopo River system. In F. Eckardt (Ed.), *Landforms and Landscapes of Botswana* (pp. 287–298). Cham: Springer. https://doi.org/10.1007/978-3-030-86102-5_16

Knight, J., & Evans, M. (2017). The sediment stratigraphy of a flood event: An example from the Sabie river, South Africa. *Catena*, *151*, 87–97. https://doi.org/10.1016/j.catena.2016.12.015

Knight, J., & Evans, M. (2018). Luminescence dating, sediment analyses, and flood dynamics on the Sabie River, South Africa. *Geomorphology*, *319*, 1–14. https://doi.org/10.1016/j.geomorph.2018.07.011

Knight, J., & Evans, M. (2022). Characterising the dynamics of river systems: An example of the Sabie River, South Africa. *Koedoe*, *64*(1), a1700. https://doi.org/10.4102/koedoe.v64i1.1700

Knight, J., & Grab, S. W. (2018). Drainage network morphometry and evolution in highland eastern Lesotho, southern Africa. *Quaternary International*, *470*, 4–17. https://doi.org/10.1016/j.quaint.2017.07.024

Larkin, Z. T., Tooth, S., Ralph, T. J., Duller, G. A. T., McCarthy, T., Keen-Zebert, A., & Humphries, M. S. (2017). Timescales, mechanisms, and controls of incisional avulsions in floodplain wetlands: Insights from the Tshwane River, semiarid South Africa. *Geomorphology*, *283*, 158–172. https://doi.org/10.1016/j.geomorph.2017.01.021

Li, K., Qin, J., Chen, J., Shen, J., & Li, S.-H. (2021). Multi-method luminescence dating of old fluvial sediments from northern Tian Shan, China. *Geochronometria*, *48*(1), 339–350. https://doi.org/10.2478/geochr-2020-0014

Mahan, S. A., Rittenour, T. M., Nelson, M. S., Ataee, N., Brown, N., DeWitt, R., Durcan, J., Evans, M., Feathers, J., Frouin, M., Guérin, G., Heydari, M., Huot, S., Jain, M., Keen-Zebert, A., Li, B., López, G. I., Neudorf, C. . . . Thomsen, K. (2023). Guide for interpreting and reporting luminescence dating results. *GSA Bulletin*, *135*(5–6), 1480–1502. https://doi.org/10.1130/B36404.1

Maswanganye, S. E., Dube, T., Mazvimavi, D., & Jovanovic, N. (2022). Remotely sensed applications in monitoring the spatio-temporal dynamics of pools and flows along non-perennial rivers: A review. *South African Geographical Journal*, *104*(4), 427–445. https://doi.org/10.1080/03736245.2021.1967774

Milan, D., Heritage, G., Entwistle, N., & Tooth, S. (2018b). Morphodynamic simulation of sediment deposition patterns on a recently stripped bedrock anastomosed channel. *IAHS Publication*, *377*, 51–56. https://doi.org/10.5194/piahs-377-51-2018

Milan, D., Heritage, G., Tooth, S., & Entwistle, N. (2018a). Morphodynamics of bedrock-influenced dryland rivers during extreme floods: Insights from the Kruger National Park, South Africa. *GSA Bulletin*, *130*(11–12), 1825–1841. https://doi.org/10.1130/B31839.1

Milan, D. J., Tooth, S., & Heritage, G. L. (2020). Topographic, hydraulic, and vegetative controls on bar and island development in mixed bedrock-alluvial, multichanneled, dryland rivers. *Water Resources Research*, *56*(5), e2019WR026101. https://doi.org/10.1029/2019WR026101

Moon, B. P., & Heritage, G. L. (2001). The contemporary geomorphology of the Letaba River in the Kruger National Park. *Koedoe*, *44*(1), 45–55. https://doi.org/10.4102/koedoe.v44i1.185

Murray, A. S., & Wintle, A. G. (2000). Luminescence dating of quartz using an improved single-aliquot regenerative-dose protocol. *Radiation Measurements*, *32*(4–5), 57–73. https://doi.org/10.1016/S1350-4487(99)00253-X

Murray, A. S., & Wintle, A. G. (2003). The single aliquot regenerative dose protocol: Potential for improvements in reliability. *Radiation Measurements*, *37*(4–5), 377–381. https://doi.org/10.1016/S1350-4487(03)00053-2

Prescott, J. R., & Hutton, J. T. (1994). Cosmic ray contributions to dose rates for luminescence and ESR dating: Large depths and long-term time variations. *Radiation Measurements*, *23*(2–3), 497–500. https://doi.org/10.1016/1350-4487(94)90086-8

Rountree, M. W., Rogers, K. H., & Heritage, G. L. (2000). Landscape state change in the semi-arid Sabie River, Kruger National Park, in response to flood and drought. *South African Geographical Journal*, *82*(3), 173–181. https://doi.org/10.1080/03736245.2000.9713711

Rowntree, K. M., & Wadeson, R. A. (1999). *A hierarchical framework for categorising the geomorphology of river systems*. Water Research Commission Report 497/1/99, Pretoria: WRC,

Rowntree, K. M., Wadeson, R. A., & O'Keeffe, J. (2000). The development of a geomorphological classification system for the longitudinal zonation of South African rivers. *South African Geographical Journal*, *82*(3), 163–172. https://doi.org/10.1080/03736245.2000.9713710

Saraiva Okello, A. M. L., Masih, I., Uhlenbrook, S., Jewitt, G. P. W., van der Zaag, P., & Riddell, E. (2015). Drivers of spatial and temporal variability of streamflow in the Incomati river basin. *Hydrology and Earth System Sciences*, *19*(2), 657–673. https://doi.org/10.5194/hess-19-657-2015

Schutte, I. C. (1986). The general geology of the Kruger National Park. *Koedoe*, *29*(1), 13–37. https://doi.org/10.4102/koedoe.v29i1.517

State of the Rivers Report. (2001). *Letaba and Luvuvhu river systems*. Pretoria: Water Research Commission, WRC report TT 165/01.

Thompson, C., Rhodes, E., & Croke, J. (2007). The storage of bed material in mountain stream channels as assessed using Optically Stimulated Luminescence dating. *Geomorphology*, *83*(3–4), 307–321. https://doi.org/10.1016/j.geomorph.2006.02.020

Toone, J., Rice, S. P., & Piégay, H. (2014). Spatial discontinuity and temporal evolution of channel morphology along a mixed bedrock-alluvial river, upper Drôme River, southeast France: Contingent responses to external and internal controls. *Geomorphology*, *205*, 5–16. https://doi.org/10.1016/j.geomorph.2012.05.033

Tooth, S., Rodnight, H., Duller, G. A. T., McCarthy, T. S., Marren, P. M., & Brandt, D. (2007). Chronology and controls of avulsion along a mixed bedrock-alluvial river. *GSA Bulletin*, *119*(3–4), 452–461. https://doi.org/10.1130/B26032.1

Venter, F. J. (1986). Soil patterns associated with the major geological units of the Kruger National Park. *Koedoe*, *29*(1), 125–138. https://doi.org/10.4102/koedoe.v29i1.525

Walsh, E. V., Burrough, S. L., & Thomas, D. S. G. (2023). A chronological database assessing the late quaternary palaeoenvironmental record from fluvial sediments in southwestern Africa. *Earth-Science Reviews*, *236*, 104288. https://doi.org/10.1016/j.earscirev.2022.104288

Wohl, E., & Beckman, N. D. (2014). Leaky rivers: Implications of the loss of longitudinal fluvial disconnectivity in headwater streams. *Geomorphology*, *205*, 27–35. https://doi.org/10.1016/j.geomorph.2011.10.022

Yanites, B. J. (2018). The dynamics of channel slope, width, and sediment in actively eroding bedrock river systems. *Journal of Geophysical Research: Earth Surface*, *123*(7), 1504–1527. https://doi.org/10.1029/2017JF004405